Rayleigh–Bloch Waves in CMUT Arrays

Abdullah Atalar, *Fellow, IEEE*, Hayrettin Köymen, *Senior Member, IEEE*, and H. Kağan Oğuz, *Student Member, IEEE*

***Abstract*—Using the small-signal electrical equivalent circuit of a capacitive micromachined ultrasonic transducer (CMUT) cell, along with the self and mutual radiation impedances of such cells, we present a computationally efficient method to predict the frequency response of a large CMUT element or array. The simulations show spurious resonances, which may degrade the performance of the array. We show that these unwanted resonances are due to dispersive Rayleigh–Bloch waves excited on the CMUT surface–liquid interface. We derive the dispersion relation of these waves for the purpose of predicting the resonance frequencies. The waves form standing waves at frequencies where the reflections from the edges of the element or the array result in a Fabry-Pérot resonator. High-order resonances are eliminated by a small loss in the individual cells, but low-order resonances remain even in the presence of significant loss. These resonances are reduced to tolerable levels when CMUT cells are built from larger and thicker plates at the expense of reduced bandwidth.**

I. Introduction

Capacitive micromachined ultrasonic transducers (CMUTs) are wideband transducers [1] with very low loss. Because individual CMUT cells are small, in practice many of them are connected in parallel to form larger transducers. Crosstalk between the cells of an array has been of considerable interest [2]. The artifacts observed in the point spread function of CMUT arrays were attributed to crosstalk between the elements [3]. The spurious responses were believed to be due either to Stoneley waves [4] in the interface or to Lamb waves [5] in the substrate. Scholte [6] waves traveling in the interface between the array surface and the immersion medium were also held responsible. Using finite element models and optical displacement measurements, acoustic coupling through the fluid medium was found to be the major source of cross-coupling between the elements [2]. Dummy elements on the substrate or reflections from the edges of the substrate also introduced unwanted responses [4].

Eccardt *et al.* [7] described a dispersive surface wave on CMUT arrays by considering infinitesimally small CMUT cells. They derived an analytical expression that defines the phase velocity of the surface waves as a function of frequency. Analysis of infinitely large CMUT arrays was carried out using an impedance matrix and the Fourier transform method [8]. The results indicated the presence of parasitic surface waves, which may be damped by resistors in series with each CMUT cell. A spectral finite element analysis/boundary element method was used to predict the response of infinite quasi-periodic CMUT structures for the purpose of finding dispersion characteristics of possible parasitic waves like leaky Rayleigh, Stoneley–Scholte, and Lamb waves [9]. The method predicted the presence of a slow dispersive wave at low frequencies caused by cross-talk between the cells with a cut-off frequency determined by cell pitch. This spurious surface wave was used as a sensor of fluid viscosity [10].

The acoustic mutual coupling between the cells and the response of a single cell were combined in a small-signal model to simulate the response of five CMUT cells using a piston radiator assumption, indicating an uneven response [11]. A small-signal analytical method covering a selected number of higher order plate modes was implemented to predict the response of a group of CMUTs [12]. The number of unknowns is equal to the number of cells multiplied by the number of CMUT plate modes. The mutual impedance between the cells was calculated numerically from the Rayleigh integral. Limited by the computation time, the mutual impedance was ignored beyond a relatively small radius. The method was able to predict coupling between different plate modes in a seven-cell CMUT configuration. The response of a CMUT array containing 1280 cells was also computed, indicating sharp peaks in the low-frequency response [13].

In this paper, we first present a computationally efficient method to simulate large CMUT elements or arrays containing thousands of cells. We employ a small-signal equivalent circuit of an individual cell modeling only the lowest order mode of the CMUT plate, hence the number of unknowns is equal to just the number of cells. The mutual radiation impedances in the immersion medium between all cells are included using an analytical approximation. Our method is accurate at low frequencies when the coupling between the cells is strong, but it does not predict the response at high frequencies where the higher order modes are excited. We show that the spurious resonances observed at low frequencies are due to Rayleigh–Bloch waves excited on the surface of the elements or arrays.

II. Single CMUT Cell in Immersion

Let us consider a circular full-electrode single CMUT cell as shown in Fig. 1.

The immersed CMUT can be represented by an electrical equivalent circuit [14] as shown in Fig. 2. This simple

Manuscript received July 1, 2014; accepted September 29, 2014.

A. Atalar and H. Köymen are with the Department of Electrical and Electronics Engineering, Bilkent University, Ankara, Turkey (e-mail: atalar@ee.bilkent.edu.tr).

H. K. Oğuz is with the Department of Electrical Engineering, Stanford University, Stanford, CA.

DOI http://dx.doi.org/10.1109/TUFFC.2014.006610

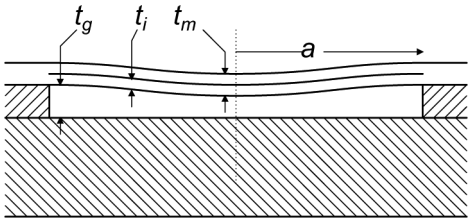

Fig. 1. Cross-sectional view of a CMUT cell of radius a with full electrode.

linear circuit only models the lowest order vibrational mode of the CMUT plate under small-signal regime; it does not predict the response at higher frequencies where higher order modes may be excited or for large signals where harmonics will be generated. The parameters of the circuit model are defined in the Appendix for completeness. A series resistor, R_{A}, is inserted in the mechanical side to take care of the mechanical loss.

III. Response of an Array of N Cells

Consider an array of m elements, each containing n identical CMUT cells, with a total of $N = mn$ cells that are arbitrarily placed in a flat rigid baffle and are immersed in liquid. Referring to Fig. 3, the mechanical ports of the cells are connected to an N-port represented by the $\mathbf{Z}$ matrix, which accounts for the self and mutual radiation impedances of the cells.[1] For generality, the electrical port of each CMUT cell contains a series resistor, R_{S}. The array elements are connected to the voltage sources represented by the phasors, $V_{\mathrm{in}1}, V_{\mathrm{in}2}, \ldots, V_{\mathrm{in}m}$, all with source impedances of R_{T}.

To solve the cell velocities, v_p, for $p = 1, 2, \ldots, N$, we write

$$n_{\mathrm{R}} V_p = \left[j\omega L_{\mathrm{R}m} + \frac{1}{j\omega}\left(\frac{1}{C_{\mathrm{R}m}} - \frac{1}{C_{\mathrm{RS}}} \right) + R_{\mathrm{A}} + Z_{\mathrm{RR}}(ka) \right] v_p + \sum_{q=1 \, q \neq p}^{N} Z_{\mathrm{M}}(ka, kd_{pq}) v_q. \tag{1}$$

This set of N equations can be written in matrix form as

$$n_{\mathrm{R}} \mathbf{V} = \mathbf{M}(\omega)\mathbf{v}, \tag{2}$$

where $\mathbf{V}$ and $\mathbf{v}$ are column vectors of the voltages, V_p, and the velocities, v_p, for $p = 1, 2, \ldots, N$, respectively. $\mathbf{M}(\omega)$ is an $N \times N$ square matrix with the entries defined as in (1). With $\mathbf{i}$ being defined as an $N \times 1$ column vector of currents $i_1, i_2, \ldots, i_N$, we write

$$\mathbf{i} = j\omega C_{0d} \mathbf{V} + n_{\mathrm{R}} \mathbf{v}. \tag{3}$$

[1] Z is a full matrix because the mutual radiation impedance function is a slowly decaying function of separation.

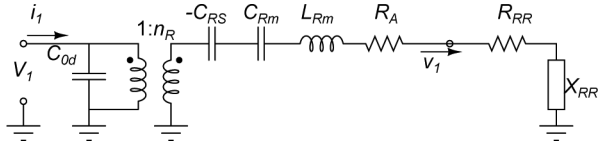

Fig. 2. Small-signal equivalent circuit of an immersed CMUT cell.

If $\mathbf{V_E}$ is an $N \times 1$ column vector of element voltages with appropriate entries equal to $V_{\mathrm{E}1}$, $V_{\mathrm{E}2}$, …, or $V_{\mathrm{E}m}$, we have

$$\mathbf{V_E} = R_{\mathrm{S}}\mathbf{i} + \mathbf{V}. \tag{4}$$

Finally, we express $\mathbf{V_{in}}$, an $N \times 1$ column vector of drive voltages with corresponding entries equal to $V_{\mathrm{in}1}$, $V_{\mathrm{in}2}$, …, or $V_{\mathrm{in}m}$, as

$$\mathbf{V_{in}} = R_{\mathrm{T}}\mathbf{J}\mathbf{i} + \mathbf{V_E}, \tag{5}$$

where $\mathbf{J}$ is an $N \times N$ matrix, which contains m all-ones matrices ($n \times n$ each) along its diagonal to add the currents of the cells appropriately. Combining the matrix equations (2)–(5), we reach

$$n_{\mathrm{R}} \mathbf{V_{in}} = \mathbf{\Psi}(\omega)\mathbf{v} \quad \text{with} \tag{6}$$

$$\mathbf{\Psi}(\omega) = [j\omega C_{0d}(R_{\mathrm{T}}\mathbf{J} + R_{\mathrm{S}}\mathbf{I}) + \mathbf{I}]\mathbf{M} + n_{\mathrm{R}}^2(R_{\mathrm{T}}\mathbf{J} + R_{\mathrm{S}}\mathbf{I}), \tag{7}$$

where the $\mathbf{I}$ is an $N \times N$ identity matrix. Hence, the cell velocities, $\mathbf{v}$, can be found at ω by the inversion of the $N \times N$ $\mathbf{\Psi}(\omega)$ matrix. For an 80×240 array with 48 elements ($m = 48$, $n = 400$), the $\mathbf{\Psi}$ matrix of $19\,200 \times 19\,200$ needs to be inverted. If a symmetry exists, the size of the matrix can be reduced.

Once the velocities of the individual cells, $\mathbf{v}$, have been found, the input currents of elements, $i_{\mathrm{in}1}$, $i_{\mathrm{in}2}$, …, $i_{\mathrm{in}m}$, defined by $\mathbf{i_{in}}$ column vector can be determined from (2) and (3):

$$\mathbf{i_{in}} = \mathbf{J}\left(\frac{j\omega C_{0d}}{n_{\mathrm{R}}} \mathbf{M}(\omega) + n_R \mathbf{I} \right) \mathbf{v}. \tag{8}$$

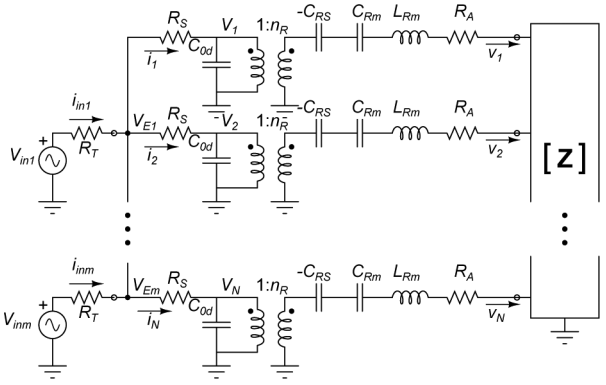

Fig. 3. Small-signal equivalent circuit of an array of CMUT cells immersed in a liquid medium. Elements are driven by ac voltage sources, $V_{\mathrm{in}1}, \ldots, V_{\mathrm{in}m}$, each with a source resistance R_{T}. A resistor, R_{S}, is placed in series with each cell.

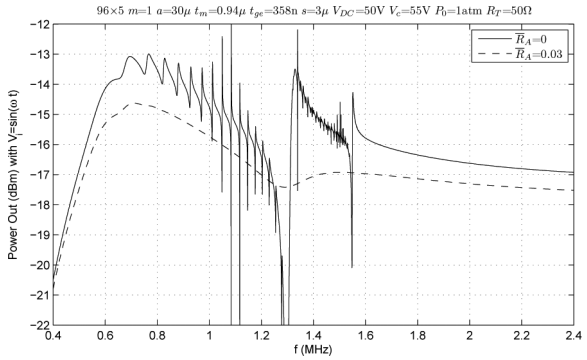

Fig. 4. Acoustic power delivered by a single array element ($m = 1$, $N = n = 96 \times 5 = 480$) of size (defined in water at 2 MHz) as a function of frequency. The cells have a radius of 30 μm with no loss ($\bar{R}_{\mathrm{A}} = 0$, solid line) and with a 0.6 dB loss ($\bar{R}_{\mathrm{A}} = 0.03$, dashed line) are placed in a rectangular pattern.

Hence, the absolute acoustic power output, P_{out}, delivered to the liquid medium can be found as the power input minus the power dissipated on resistors R_{A}, R_{T}, and R_{S} as follows:

$$P_{\mathrm{out}} = \frac{1}{2}\sum_{p=1}^{m}\mathrm{Re}\{V_{\mathrm{in}p}\, i_{\mathrm{in}p}^{*}\} - \frac{1}{2}R_{\mathrm{A}}\sum_{p=1}^{N}|v_p|^2 - \frac{1}{2}R_{\mathrm{T}}\sum_{p=1}^{m}|i_{\mathrm{in}p}|^2 - \frac{1}{2}R_{\mathrm{S}}\sum_{p=1}^{N}|i_p|^2. \tag{9}$$

We developed a Matlab (The MathWorks Inc., Natick, MA) code utilizing array operations to make use of multicore processors. The code is optimized so that matrix inversion determines the execution time, while the matrix-fill time is a small fraction. It is verified with the results of our earlier simulations [15] which used a harmonic balance simulator. In all simulations that follow, the cell dimensions are adjusted so that they have a collapse voltage of $V_{\mathrm{c}} = 55$ V under 1 atm = 101.3 kPa pressure and a single-cell resonance frequency of 1.4 MHz in water. The elements are driven by a sinusoidal unit voltage source of $R_{\mathrm{T}} = 50\ \Omega$ resistance with $R_{\mathrm{S}} = 0$, and CMUT cells are biased with $V_{\mathrm{DC}} = 50$ V.[2]

A. Single-Array Element Simulations

The cells of dimensions $a = 30$ μm, $t_m = 0.94$ μm, and $t_{\mathrm{ge}} = 358$ nm are placed in a rectangular grid of 96×5 in a single element with a cell-to-cell separation of $s = 3$ μm. Initially, the mechanical loss resistor, R_{A}, is assumed to be zero. The solid curve in Fig. 4 shows the acoustic power output calculated from (9) as a function of frequency. Note the presence of spurious resonances for frequencies lower than 1.6 MHz.

[2]We use $Y_0 = 320$ GPa, $\sigma = 0.263$, $\rho = 3270$ kg/m^3, $c_0 = 1500$ m/s, and $\rho_0 = 1000$ kg/m^3, unless noted otherwise. Available power from the source is 4 dBm.

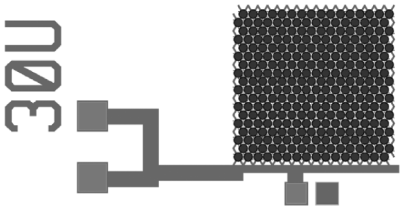

Fig. 5. Layout of a CMUT element with hexagonally packed 18×16 cells. The cells have Si_3N_4 plates with dimensions $a = 30$ μm, $s = 6$ μm, $t_m = 1.88$ μm, $t_q = 70$ nm, $t_i = 160$ nm, and material constants are $Y_0 = 140$ GPa, $\rho = 3100$ kg/m^3, $\sigma = 0.27$, $\varepsilon_r = 5.4$.

Losses present in the CMUT cells can cause the spurious resonances to disappear [8]. The loss can be introduced by adding a series resistor to each cell [16] (R_{S}) or by adding a lossy layer on top of the CMUT cells [17] at the mechanical side. The effect of the mechanical loss can be investigated by using a nonzero value for R_{A}.[3] The dashed curve in Fig. 4 presents the calculated power output of the same element, with $\bar{R}_{\mathrm{A}} = R_{\mathrm{A}}/\rho_0 c_0 \pi a^2 = 0.03$ resulting in about 0.6 dB reduction in the output power. The calculated curves are similar to experimentally measured responses of arrays [4], [18], [19]. This damping gets rid of the high-Q resonances, but remnants of some resonances are still there.

We note that it is relatively difficult to introduce a loss in the electrical side. Because the individual CMUTs have high electrical impedance, a series resistor (R_{S}) for each cell on the order of 100 kΩ is necessary to introduce a significant loss.

Fig. 5 shows the layout of a CMUT element with 18×16 hexagonally packed cells. The devices were fabricated [20] with a low-temperature surface micromachining technology utilizing a Cr sacrificial layer and Si_3N_4 deposition by a plasma-enhanced chemical vapor deposition system. The electrical impedance measurements are carried out using a 50-Ω network analyzer. Fig. 6 depicts a comparison of calculated and measured conductances[4] of the element under different bias voltages. The spurious resonance frequencies are predicted very well, verifying the validity of the model.

B. Array Simulations

We simulate a 1-D linear array with 48 elements made up of cells with $a = 36.3$ μm.[5] Each element contains 80×5 rectangularly placed cells with a separation of $s = 3$ μm. Elements are driven at 0.70 MHz by linearly increasing delays of 0, 1/8, 2/8, …, 47/8 μs ($\Delta = 1/8$ μs) to simulate a case where the beam is steered at an angle

[3]The resistor R_{A} may well have a frequency dependence, but we assume it to be independent of frequency.

[4]A square-law frequency-dependent conductance due to the loss in the insulator layer at zero bias is subtracted from the measured conductances.

[5]$t_m = 1.31$ μm, $t_{\mathrm{ge}} = 325$ nm to satisfy $V_c = 55$ V and a single cell resonance at 1.4 MHz.

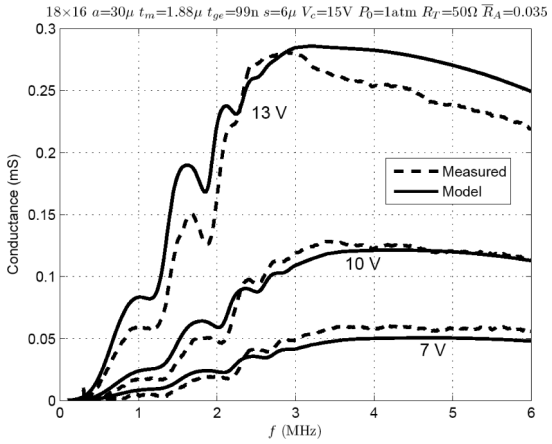

Fig. 6. Calculated (solid) and measured (dashed) conductances of the 18 × 16 element immersed in sunflower oil with bias voltages of $V_{\mathrm{DC}} = 7$, 10, and 13 V. The constants of vegetable oil are $c_0 = 1450$ m/s and $\rho_0 = 915$ kg/m^3. The loss resistance of CMUTs is selected as $\overline{R}_{\mathrm{A}} = 0.035$ for a good fit.

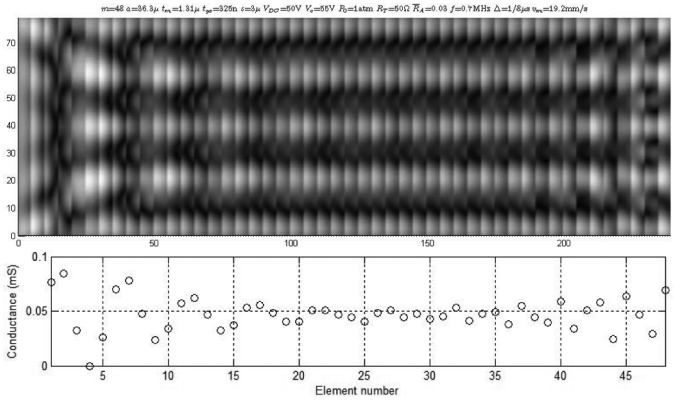

Fig. 7. Upper graph: Calculated velocity magnitude map of an array of 80 × 240 cells divided to 48 elements (each element is about $2.8\lambda \times 0.17\lambda$ with λ defined in water) at 0.70 MHz. Lower graph: Conductance of elements. The cells have a radius of 36.3 μm with 0.6 dB loss and are placed in a rectangular pattern. Elements are excited with increasing delays ($\Delta = 1/8$ μs).

of $\theta = 30°$ with respect to the normal. The calculated cell velocity distribution is shown in Fig. 7 as a grayscale map demonstrating uneven velocities within the elements and the array. The electrical conductances of the elements are also shown in the same figure, indicating a large variation between the elements.

Next, we simulate another 1-D linear array with sixty-four elements made up of cells with 26% larger cells: $a = 45.7$ μm.[6]

The elements are driven by equal voltages with linearly increasing delays: 0, 1/8, 2/8, …, 63/8 μs ($\Delta = 1/8$ μs). The velocity magnitudes of individual cells obtained from (6) with $\overline{R}_{\mathrm{A}} = 0.03$ are shown in Fig. 8 at different frequencies showing a considerable nonuniformity in cell velocities.[7] Fig. 9 shows the plots of the velocity distribution along selected columns of the same array at the same frequencies, quantitatively depicting the uneven velocity distribution. Note that the nature of nonuniformity is different at 2 MHz, where the velocity fluctuation is minimal within a column, but substantial among different columns of the same element.

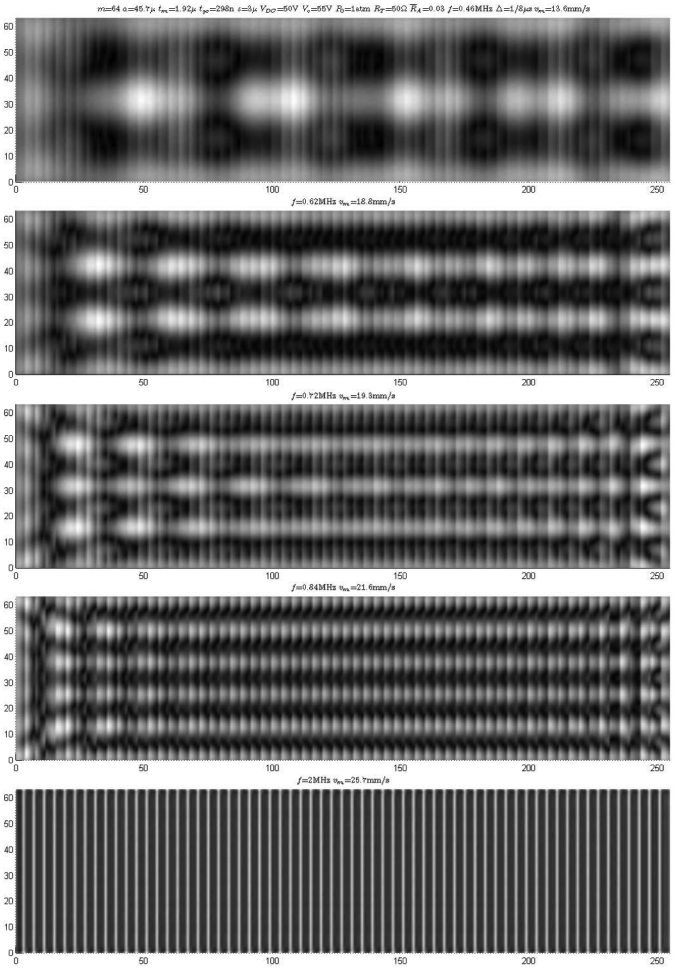

Fig. 8. Calculated CMUT velocity magnitude distribution of a 64 × 256 array ($N = 16384$) with sixty-four elements ($m = 64$) made up of rectangularly packed cells with radius $a = 45.7$ μm with 0.6 dB loss at 0.46, 0.62, 0.72, 0.84, and 2.00 MHz. v_{m} is the maximum velocity in each graph. Elements of 64 × 4 cells are approximately $8\lambda \times \lambda/2$ in size, where λ is defined in water at 2 MHz and they are excited with increasing delays to steer the beam at $\theta = 30°$ with respect to the normal ($\Delta = 1/8$ μs).

IV. Normalized Velocity Fluctuation

To compactly quantify the amount of fluctuation in the velocities, we define a normalized velocity fluctuation, $\tilde{v}$, within the array using the absolute value of the deviation from the average velocity as a function of frequency:

$$\tilde{v}(f) = \frac{1}{N|\overline{v}|_{\max}} \sum_{p=1}^{N} \left| |v_p(f)| - \overline{|v(f)|} \right|, \qquad (10)$$

[6] $t_m = 1.92$ μm, $t_{\mathrm{ge}} = 298$ nm to maintain the same V_c and the same resonance frequency.

[7] Computation time for the array of 64 × 256 cells ($N = 16384$) is 350 s per frequency point on an Intel i7-4800MQ CPU (Intel Corp., Santa Clara, CA) running at 2.7 GHz clock.

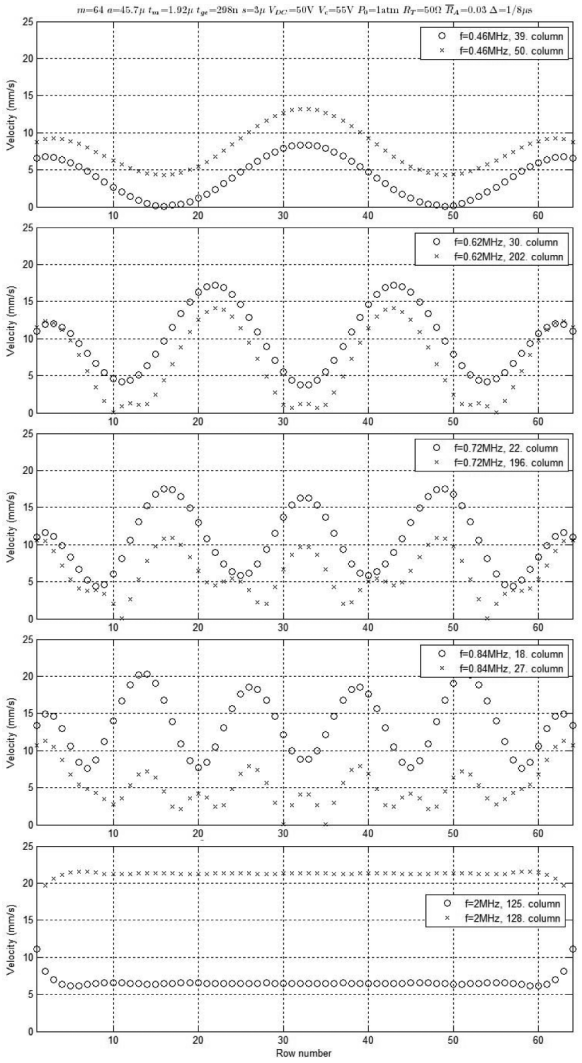

Fig. 9. Calculated CMUT cell velocity magnitude distribution along selected columns of the 64 × 256 array of Fig. 8 at 0.46, 0.62, 0.72, 0.84, and 2.00 MHz.

where $\overline{|v(f)|}$ is the average velocity amplitude within the array of N cells at frequency f, and normalization factor $\overline{|v|}_{\max}$ is the average velocity at the center frequency. $\tilde{v} = 0$ means that all cells move with the equal amplitude within the array, whereas a nonzero value of $\tilde{v}$ imply a variation in the velocities of cells within the array. Fig. 10 shows calculated values of $\tilde{v}$ of the array of Section III-B as a function of frequency. The spurious resonances are seen as peaks in the graph. The same graph also shows $\tilde{v}$ while the acoustic loss is increased. A higher acoustic loss reduces the fluctuation as expected. Fig. 11 is a similar graph when the delays between the excitations of neighboring elements are varied. As the delay, Δ, is increased (resulting in a higher steering angle, θ), the fluctuation increases, especially at frequencies higher than the resonant frequency of the single cell. The lowest fluctuation occurs when all elements are excited with the same voltage.

To see the effect of CMUT cell parameters on the $\tilde{v}$ performance, we simulated two more arrays with larger

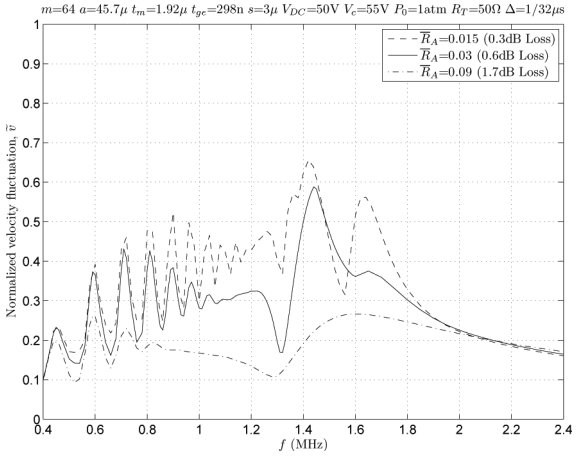

Fig. 10. Calculated normalized velocity fluctuation ($\tilde{v}$) within the array of Fig. 8 as a function of frequency for various acoustic loss levels of 0.3, 0.6, and 1.7 dB ($\overline{R}_{\mathrm{A}} = 0.015$, 0.03, 0.09). $\overline{|v|}_{\max}$ is defined at 2 MHz.

and thicker plates with the same resonance frequency (1.4 MHz) and collapse voltage (55 V). The first one has medium-size CMUT cells: $a = 94.2$ μm, $t_m = 6.4$ μm, $t_{\mathrm{ge}} = 227$ nm. The radius of the cells is about two times larger, hence an array with the same area is obtained with 32 × 128 cells. Each of the 64 elements contains 32 × 2 cells. Fig. 12 depicts the performance of the array as a function of frequency for different delays between consecutive array elements. The fluctuation is somewhat reduced, but it is still relatively high. The second array (16 × 64) contains even larger CMUT cells with $a = 189.9$ μm, $t_m = 23.9$ μm, $t_{\mathrm{ge}} = 150$ nm, where the elements are made from 16 × 1 cells. Fig. 13 shows $\tilde{v}$ for this array of the same overall size. As the CMUT cells are made larger, $\tilde{v}$ is considerably reduced. For comparison, the acoustic power outputs of the three arrays are plotted in Fig. 14 as a function of frequency. Note that the power output of the array with largest cells is 11 dB higher than that with the smallest cells at the center frequency because of a better impedance match at the expense of reduced bandwidth.

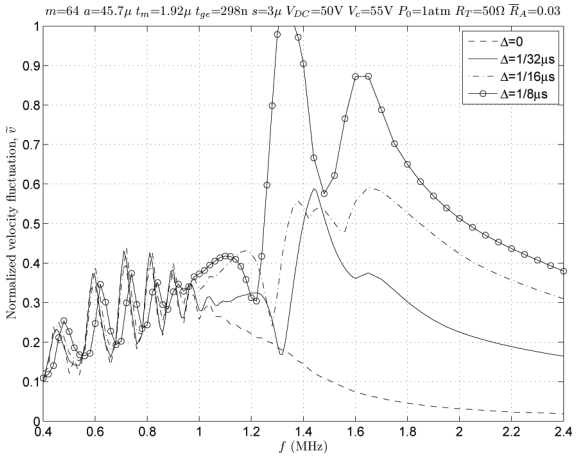

Fig. 11. Calculated normalized velocity fluctuation ($\tilde{v}$) within the array of Fig. 8 as a function of frequency for various delays between neighboring cells, corresponding to 0°, 7°, 14°, and 30° steering angles.

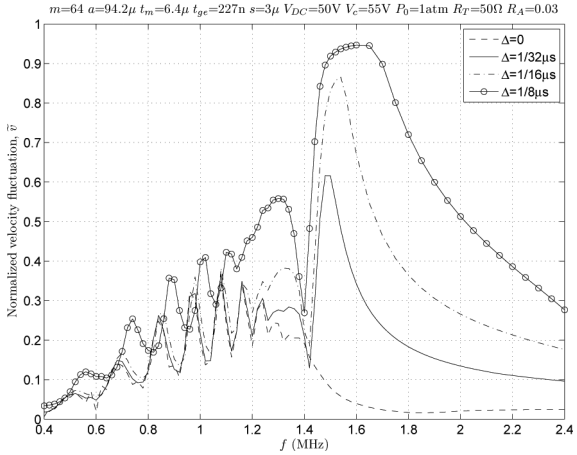

Fig. 12. Calculated normalized velocity fluctuation ($\bar{v}$) within a same size 32×128 array built from medium size cells as a function of frequency for various delays between neighboring cells.

V. Dispersive Rayleigh–Bloch Waves

It is known that periodically placed resonators support surface waves known as Rayleigh–Bloch (R-B) waves [21]. Linton and McIver [22] showed that these waves can exist along the surface of periodic structures in the absence of any incident waves. It was pointed out that R-B waves can exist on the CMUT–fluid interface [8]. These waves exist along the periodic structure surface with no leakage into the surrounding medium, because their phase velocity is slower than that of a bulk wave in the liquid medium. The dispersive surface wave detected on the surface of infinite CMUT structures [9] is the R-B wave.

To find the characteristics of the possible R-B waves, we follow the approach of Collin [23] and consider an infinite element of CMUT cells with no mechanical loss. As an example, we consider two infinite rows of CMUT cells as shown in Fig. 15, all driven in parallel with an ac voltage source of V_{in} (with $R_{\text{T}} = 0$). Let d represent the distance between the centers of the neighboring cells.

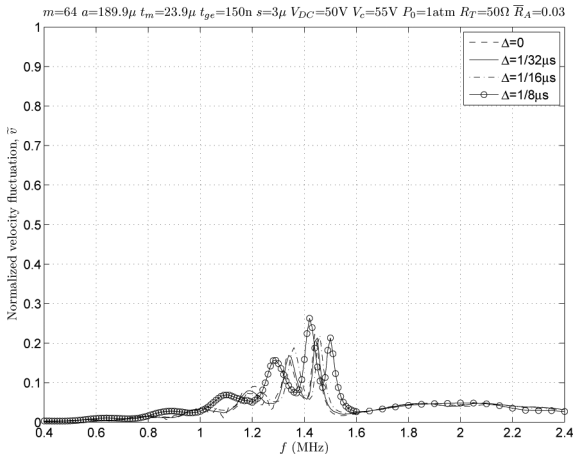

Fig. 13. Calculated normalized velocity fluctuation ($\bar{v}$) within a same size 16×64 array built from large size cells as a function of frequency for various delays between neighboring cells.

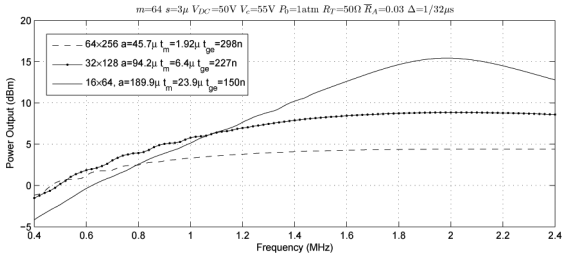

Fig. 14. Calculated acoustic power outputs of the three arrays of the same overall size as a function of frequency. The total available power from the electrical side is 22 dBm, indicating a center-frequency conversion loss of 17.5, 13, and 6.5 dB, respectively.

We assume that an R-B wave exists, propagating in the x-direction with a phase velocity of v_{B}. (It is not possible to support an R-B wave in the y-direction because of symmetry.) We represent this interface wave by $e^{-j(\omega/v_{\text{B}})x}$. Because of the infinite geometry, the surface wave amplitude must have no x dependence. Therefore, all cells must vibrate with the same plate velocity, v_1, except for the phase factor given by $e^{-j(\omega/v_{\text{B}})x}$, where x is the position of the cell center. For any cell, we can write the following equation, which includes the mechanical and self-radiation impedance of the cell as well as the mutual impedance of all the other cells:

$$n_{\text{R}} V_{\text{in}} = \Psi(\omega) v_1 \tag{11}$$

$$\Psi(\omega) = \left\{ j\omega L_{\text{R}m} + \frac{1}{j\omega} \frac{C_{\text{RS}} - C_{\text{R}m}}{C_{\text{R}m} C_{\text{RS}}} + Z_{\text{RR}}(ka) + Z_{\text{M}}(ka, kd) + \sum_{q=1}^{N\to\infty} \left[\left(e^{-j(\omega/v_{\text{B}})qd} + e^{j(\omega/v_{\text{B}})qd} \right) \cdot \left(Z_{\text{M}}(ka, kdq) + Z_{\text{M}}(ka, kd\sqrt{q^2+1}) \right) \right] \right\}. \tag{12}$$

The exponential factors in the infinite summation of Ψ account for the phase differences of the neighboring cells with x-separation of qd on the left and on the right. The factor $d\sqrt{q^2+1}$ defines the distance between the centers of the cells in the alternate rows. For a given ω, v_1 will be maximized if Ψ is minimum. This condition is met if the imaginary part of Ψ is zero. To find v_{p} in terms of ω, we can write this condition as the dispersion relation:

$$\text{Im}\{\Psi(\omega)\} = 0. \tag{13}$$

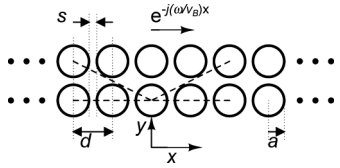

Fig. 15. Geometry of two infinite rows of CMUT cells. Dashed lines show the distances to neighboring cells for $q = 2$ in (12): $2d$ and $d\sqrt{2^2+1}$.

TABLE I. SOME RESONANCE FREQUENCIES AND Q FACTORS OF THE 2×44 CMUT ELEMENT FOUND USING (15) AND (16).

f_0 (MHz)	1.203	1.255	1.301	1.343	1.381	1.415	1.446
Q	62	212	792	4231	2020	2718	11 644
f_0 (MHz)	1.473	1.498	1.520	1.539	1.555	1.569	1.580
Q	2540	1169	830	621	479	432	393

For the purpose of numerical evaluation, the upper limit of the infinite summation in (12) is taken as N such that $Nd > 40\lambda = 40\omega/c_0$ (with λ defined at the frequency of single cell resonance). In Fig. 16(a), we plot the dispersion curve for the CMUT element of Fig. 15, composed of cells with $a = 30$ μm, $t_m = 0.94$ μm, $s = 3$ μm, and a single-cell resonance in water of 1.4 MHz. Because of symmetry, the dispersion relation is also valid for a surface wave traveling in the opposite direction ($e^{+j(\omega/v_B)x}$) with the same phase velocity.

The dispersion relation of R-B waves given by (12) and (13) is valid for the infinite element with two rows shown in Fig. 15, where all cells have the same amplitude. If the actual element length is not infinite, but sufficiently long, the dispersion relation is nearly the same. However, if the number of rows is different or if the element size is very small, the relation is modified.[8]

If the element is of finite length, the reflections of R-B waves at the edges can create Fabry–Pérot type standing waves at distinct frequencies when the element length is an integer multiple of the wavelength. Only even symmetric standing waves, shown in Fig. 9, are possible. Odd symmetric standing waves are not excited, because all CMUT cells within the element are driven equally. For an element of length D, the standing wave condition can be expressed as

$$D = p\lambda = p\frac{v_B}{f}, \quad \text{with } p = 1, 2, \ldots. \tag{14}$$

In Fig. 16(a), we also plot (14) as straight lines for $p = 3, 4, \ldots, 18$ and $D = 2709$ μm. The intersections of the straight lines with the dispersion curve give the approximate resonance frequencies of the element. Fig. 16(b) is a plot of the normalized velocity fluctuation of this 2×44 element near the spurious resonance frequencies. A comparison of Figs. 16(a) and 16(b) shows that the resonance frequencies are correctly estimated from the dispersion curve graph.

The Fabry–Pérot resonances of the array of Fig. 8 are clearly seen as standing waves in Fig. 9 and peaks in the graph of Fig. 10. Notice that a lower but significant $\tilde{v}$ exists even at frequencies higher than the cut-off frequency of R-B waves. Uneven loading of CMUT cells within an element, especially for the cells near the periphery of the element or when the neighboring elements are excited with different excitation voltages, is the reason for the nonuniformity.

The resonance frequencies can be found more accurately for a finite-size element or array by using (6). To maximize the velocities, v, the magnitude of the determinant of Ψ must be minimal. This occurs at frequencies where the imaginary part of the determinant of Ψ is zero:

$$\mathrm{Im}\{\det(\Psi(\omega))\} = 0. \tag{15}$$

Using this method, the resonance frequencies are calculated and listed in Table I. The values agree well with Fig. 16(b).

The quality factor, Q, at a resonance, ω_0, can be estimated from the quality factor of the determinant of Ψ around ω_0:

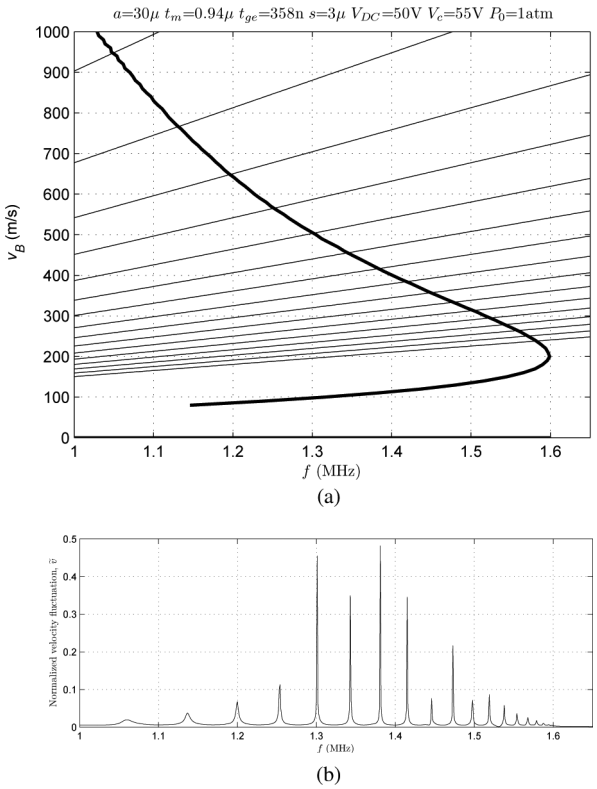

Fig. 16. (a) Dispersion curve (thick curve) for R-B waves on two infinite rows of CMUTs (Fig. 15) immersed in water. Standing wave condition of (14) is also plotted for $p = 3, 4, \ldots, 18$ and $D = 2709$ μm (thin lines). (b) Normalized velocity fluctuation of the 2×44 CMUT element with $a = 30$ μm, $t_m = 0.94$ μm, $s = 3$ μm, $D = 2709$ μm, $R_T = 0$, $R_A = 0$, and $R_S = 0$.

[8] A rearrangement of CMUT cells within the element or placement of different-sized CMUT cells in the element do not eliminate R-B waves. Such approaches simply cause a change in the dispersion curve and a shift in the spurious resonance frequencies.

$$Q = \frac{1}{2}\frac{\omega_0}{\mathrm{Re}\{\det(\Psi(\omega_0))\}}\frac{\mathrm{d}}{\mathrm{d}\omega}\mathrm{Im}\{\det(\Psi(\omega))\}\Big|_{\omega=\omega_0}. \quad (16)$$

Table I also lists these calculated values. It is seen that the highest Q values are observed around 1.4 MHz, the mechanical resonance of a single cell in water. Q drops as the frequency changes in both directions.

The dispersion curve indicates that there is a cutoff frequency (1.6 MHz in the examples) above which no R-B wave can exist. The presence of such a cutoff frequency was reported earlier from simulations [9] and experimental data [24]. Our simulations show that above 1.6 MHz, although there is a nonuniformity in the cell velocities, no standing-waves exist. This cutoff frequency was not predicted by the dispersion curve of surface waves assuming infinitesimally small CMUTs [7]. The cutoff arises from the Bragg condition when the CMUT cell pitch is equal to a half wavelength of the R-B wave. We note that the dispersion curve shown in Fig. 16(a) is only representative because it depends on the CMUT dimensions, the separation between the cells, etc. Different CMUT geometries give rise to different dispersion curves.

Our circuit theory model cannot predict the excitation of Stoneley, Scholte, or Lamb waves. It is plausible that these waves may be excited at the discontinuities of the element, such as its edges.

VI. Conclusions

We are able to simulate large arrays of CMUT cells using the small-signal equivalent circuit in a computationally efficient manner. The simulation results agree well with the experimental measurements. The spurious resonances seen around the resonance frequency of a single cell can be attributed to R-B waves present on the interface between the CMUTs and the immersion medium. They are created by the mutual interactions between the cells through the mutual radiation impedance. The resulting R-B waves are highly dispersive and have a phase velocity less than the speed of sound in the immersion medium. The spurious resonances occur when an element or array dimension is an integer multiple of the R-B wavelength. At these frequencies, there is a significant cell velocity fluctuation within an element. The inherent loss of real CMUT elements, such as the loss in the polymer protection layer, can be sufficient to eliminate some resonances. The high-order spurious resonances disappear if there is about 0.6 dB loss in the transducer, whereas the low-order resonances remain even in the presence of a significant loss factor. There is a cut-off frequency above which no R-B wave can exist. However, velocity fluctuations exist even above the cut-off frequency because of nonuniform loading of the cells, especially when the neighboring elements are excited with different voltages. If arrays are built from larger and thicker CMUT cells, the velocity variation caused by R-B waves and nonuniform loading of cells are substantially reduced at the expense of reduced bandwidth.

Appendix

A. Small-Signal RMS Equivalent Circuit of a CMUT Cell

Referring to Fig. 1, the circular CMUT cell has a radius of a, a plate thickness of t_m, and an effective gap height of $t_{\mathrm{ge}} = t_{\mathrm{g}} + t_i/\varepsilon_{\mathrm{r}}$, where ε_{r} is the relative permittivity of the insulator material. The component values of the small-signal rms equivalent circuit of Fig. 2 can be expressed as [14]

$$u = \frac{\sqrt{5}X_{\mathrm{R}}}{t_{\mathrm{ge}}} \quad \text{with } t_{\mathrm{ge}} = t_{\mathrm{g}} + t_i/\varepsilon_r \quad (17)$$

$$C_{0d} = C_0 g(u) \quad \text{with } C_0 = \frac{\varepsilon_0 \pi a^2}{t_{\mathrm{ge}}} \quad (18)$$

$$n_{\mathrm{R}} = \sqrt{5}\frac{C_0 g'(u) V_{\mathrm{DC}}}{t_{\mathrm{ge}}}, \quad L_{\mathrm{R}m} = \rho\pi a^2 t_m \quad (19)$$

$$C_{\mathrm{RS}} = \frac{2t_{\mathrm{ge}}^2}{5C_0 V_{\mathrm{DC}}^2 g''(u)}, \quad C_{\mathrm{R}m} = \frac{9}{5}\frac{(1-\sigma^2)a^2}{16\pi Y_0 t_m^3} \quad (20)$$

$$V_{\mathrm{DC}} = V_{\mathrm{r}}\sqrt{\frac{3\left(u - \frac{F_{\mathrm{Rb}}}{F_{\mathrm{Rg}}}\right)}{2g'(u)}} \quad (21)$$

$$V_{\mathrm{r}} = 8\frac{t_m^{3/2}}{a^2}t_{\mathrm{ge}}^{3/2}\sqrt{\frac{Y_0}{27\varepsilon_0(1-\sigma^2)}} \quad (22)$$

$$F_{\mathrm{Rg}} = \frac{t_{\mathrm{ge}}}{\sqrt{5}C_{\mathrm{R}m}}, \quad F_{\mathrm{Rb}} = \frac{\sqrt{5}}{3}\pi a^2 P_0 \quad (23)$$

$$\frac{V_{\mathrm{c}}}{V_{\mathrm{r}}} \approx 0.9961 - 1.0468\frac{F_{\mathrm{Rb}}}{F_{\mathrm{Rg}}} + 0.06972\left(\frac{F_{\mathrm{Rb}}}{F_{\mathrm{Rg}}} - 0.25\right)^2 + 0.01148\left(\frac{F_{\mathrm{Rb}}}{F_{\mathrm{Rg}}}\right)^6 \quad (24)$$

$$g(u) = \frac{\tanh^{-1}\sqrt{u}}{\sqrt{u}}, \quad g'(u) = \frac{1}{2u}\left(\frac{1}{1-u} - g(u)\right) \quad (25)$$

$$g''(u) = \frac{1}{2u}\left(\frac{1}{(1-u)^2} - 3g'(u)\right). \quad (26)$$

X_{R} is the static rms displacement of the plate under a bias voltage of V_{DC} and a static pressure of P_0. V_{r} and V_{c} are the collapse voltages under vacuum and under pressure P_0. Y_0, σ, and ρ are, respectively, the Young's modulus, Poisson ratio, and density of the plate material. ε_0 is the permittivity of free space.

B. Self- and Mutual Radiation Impedances of Circular CMUT Cells

Consider an immersion liquid of density ρ_0 and sound velocity c_0. For the rms equivalent circuit, the normalized

self-radiation impedance, $\overline{Z}_{\mathrm{RR}}$, of a circular CMUT cell of radius a at a wavenumber of $k = \omega/c_0$ is given [25] in terms of its real, $\overline{R}_{\mathrm{RR}}$, and imaginary, $\overline{X}_{\mathrm{RR}}$, parts in (27) and (28). The normalization factor, $\rho_0 c_0 \pi a^2$, is the radiation impedance of a piston transducer of radius a at very high frequencies. We have

$$\overline{R}_{\mathrm{RR}}(ka) = \frac{R_{\mathrm{RR}}}{\rho_0 c_0 \pi a^2} \approx 1 - 5\frac{2^{11}}{(2ka)^7} F_{122}(2ka) \tag{27}$$

$$\overline{X}_{\mathrm{RR}}(ka) = \frac{X_{\mathrm{RR}}}{\rho_0 c_0 \pi a^2} \approx -5\frac{2^{11}}{(2ka)^7} F_{222}(2ka) \tag{28}$$

for $0.1 < ka < 3$ with $k = \omega/c_0$ and

$$F_{122}(y) = y^2 J_5(y) + 2yJ_4(y) + 3J_3(y) - \frac{y^3}{16} - \frac{y^5}{768} \tag{29}$$

$$F_{222}(y) = -y^2 H_5(y) - 2yH_4(y) - 3H_3(y) + \frac{2}{\pi}\frac{y^4}{35} + \frac{2}{\pi}\frac{y^6}{945}, \tag{30}$$

where $y = 2ka$.

The mutual radiation impedance, Z_{M}, between the two cells can be approximately written as [15]

$$Z_{\mathrm{M}}(ka, kd) \approx \rho_0 c_0 \pi a^2 A(ka)\left(\frac{\sin(kd)}{kd} + j\frac{\cos(kd)}{kd}\right), \tag{31}$$

where d is the distance between the centers of the CMUT cells and

$$A(ka) = \sum_{n=0}^{10} p_n (ka)^n, \tag{32}$$

with coefficient p_i values given in [15, Table II].

References

[1] I. Ladabaum, X. Jin, H. T. Soh, A. Atalar, and B. T. Khuri-Yakub, "Surface micromachined capacitive ultrasonic transducers," *IEEE Trans. Ultrason. Ferroelectr. Freq. Control*, vol. 45, no. 3, pp. 678–690, 1998.

[2] A. Caronti, A. Savoia, G. Caliano, and M. Pappalardo, "Acoustic coupling in capacitive microfabricated ultrasonic transducers: Modeling and experiments," *IEEE Trans. Ultrason. Ferroelectr. Freq. Control*, vol. 52, no. 12, pp. 2220–2234, 2005.

[3] O. Oralkan, A. S. Ergun, J. A. Johnson, M. Karaman, U. Demirci, K. Kaviani, T. H. Lee, and B. T. Khuri-Yakub, "Capacitive micromachined ultrasonic transducers: Next-generation arrays for acoustic imaging?" *IEEE Trans. Ultrason. Ferroelectr. Freq. Control*, vol. 49, no. 11, pp. 1596–1610, 2002.

[4] X. Jin, O. Oralkan, F. L. Degertekin, and B. T. Khuri-Yakub, "Characterization of one-dimensional capacitive micromachined ultrasonic immersion transducer arrays," *IEEE Trans. Ultrason. Ferroelectr. Freq. Control*, vol. 48, no. 3, pp. 750–760, 2001.

[5] M. H. Badi, G. G. Yaralioglu, A. S. Ergun, S. T. Hansen, E. J. Wong, and B. T. Khuri-Yakub, "Capacitive micromachined ultrasonic Lamb wave transducers using rectangular membranes," *IEEE Trans. Ultrason. Ferroelectr. Freq. Control*, vol. 50, no. 9, pp. 1191–1203, 2003.

[6] J. McLean and F. L. Degertekin, "Directional Scholte wave generation and detection using interdigital capacitive micromachined ultrasonic transducers," *IEEE Trans. Ultrason. Ferroelectr. Freq. Control*, vol. 51, no. 6, pp. 756–764, 2004.

[7] P. C. Eccardt, A. Lohfink, and H. G. von Garssen, "Analysis of crosstalk between fluid coupled CMUT membranes," in *Proc. IEEE Ultrasonics Symp.*, 2005, pp. 593–596.

[8] A. Rønnekleiv, "CMUT array modeling through free acoustic CMUT modes and analysis of the fluid-CMUT interface through Fourier transform methods," *IEEE Trans. Ultrason. Ferroelectr. Freq. Control*, vol. 52, no. 12, pp. 2173–2184, 2005.

[9] M. Wilm, A. Reinhardt, V. Laude, R. Armati, W. Daniau, and S. Ballandras, "Three dimensional modelling of micromachined-ultrasonic-transducer arrays operating in water," *Ultrasonics*, vol. 43, no. 6, pp. 457–465, 2005.

[10] M. Thänhardt, P. C. Eccardt, H. Mooshofer, P. Hauptmann, and L. Degertekin, "A resonant CMUT sensor for fluid applications," in *IEEE Sensors Conf.*, 2009, pp. 878–883.

[11] C. Meynier, F. Teston, and D. Certon, "A multiscale model for array of capacitive micromachined ultrasonic transducers," *J. Acoust. Soc. Am.*, vol. 128, no. 5, pp. 2549–2561, 2010.

[12] M. Berthillier, P. Le Moal, and J. Lardiès, "Dynamic and acoustic modeling of capacitive micromachined ultrasonic transducers," in *Proc. IEEE Ultrasonics Symp.*, 2011, pp. 608–611.

[13] M. Berthillier, P. Le Moal, and J. Lardiès, "Comparison of various models to compute the vibro-acoustic response of large CMUT arrays," in *Proc. Acoustics 2012 Nantes Conf.*, pp. 3125–3130.

[14] H. Koymen, A. Atalar, E. Aydogdu, C. Kocabas, H. K. Oguz, S. Olcum, A. Ozgurluk, and A. Unlugedik, "An improved lumped element nonlinear circuit model for a circular CMUT cell," *IEEE Trans. Ultrason. Ferroelectr. Freq. Control*, vol. 59, no. 8, pp. 1791–1799, 2012.

[15] H. K. Oguz, A. Atalar, and H. Koymen, "Equivalent circuit-based analysis of CMUT cell dynamics in arrays," *IEEE Trans. Ultrason. Ferroelectr. Freq. Control*, vol. 60, no. 5, pp. 1016–1024, 2013.

[16] S. Berg, T. Ytterdal, and A. Rønnekleiv, "Co-optimization of CMUT and receive amplifiers to suppress effects of neighbor coupling between CMUT elements," in *Proc. IEEE Ultrasonics Symp.*, 2008, pp. 2103–2106.

[17] S. Berg and A. Rønnekleiv, "Reducing fluid coupled crosstalk between membranes in CMUT arrays by introducing a lossy top layer," in *Proc. IEEE Ultrasonics Symp.*, 2006, pp. 594–597.

[18] A. Caronti, G. Caliano, R. Carotenuto, A. Savoia, M. Pappalardo, E. Cianci, and V. Foglietti, "Capacitive micromachined ultrasonic transducer (CMUT) arrays for medical imaging," *Microelectron. J.*, vol. 37, no. 8, pp. 770–777, 2006.

[19] D. T. Yeh, O. Oralkan, I. O. Wygant, A. S. Ergun, J. H. Wong, and B. T. Khuri-Yakub, "High-resolution imaging with high-frequency 1-D linear CMUT arrays," in *Proc. IEEE Ultrasonics Symp.*, 2005, pp. 665–668.

[20] S. Olcum, "Deep collapse mode capacitive micromachined ultrasonic transducers," Ph.D. thesis, Electrical and Electronics Engineering Dept., Bilkent University, 2010.

[21] R. Porter and D. V. Evans, "Rayleigh–Bloch surface waves along periodic gratings and their connection with trapped modes in waveguides," *J. Fluid Mech.*, vol. 386, no. 1, pp. 233–258, 1999.

[22] C. M. Linton and M. McIver, "The existence of Rayleigh–Bloch surface waves," *J. Fluid Mech.*, vol. 470, no. 1, pp. 85–90, 2002.

[23] R. E. Collin, *Foundations for Microwave Engineering*. New York, NY: McGraw-Hill, 1992.

[24] B. Bayram, M. Kupnik, G. G. Yaralioglu, O. Oralkan, A. S. Ergun, D. S. Lin, S. H. Wong, and B. T. Khuri-Yakub, "Finite element modeling and experimental characterization of crosstalk in 1-D CMUT arrays," *IEEE Trans. Ultrason. Ferroelectr. Freq. Control*, vol. 54, no. 2, pp. 418–430, 2007.

[25] M. N. Senlik, S. Olcum, H. Koymen, and A. Atalar, "Radiation impedance of an array of circular capacitive micromachined ultrasonic transducers," *IEEE Trans. Ultrason. Ferroelectr. Freq. Control*, vol. 57, no. 4, pp. 969–976, 2010.

Abdullah Atalar received the B.S. degree from the Middle East Technical University, Ankara, Turkey, in 1974, and M.S. and Ph.D. degrees from Stanford University, Stanford, CA, in 1976 and 1978, respectively, all in electrical engineering. He worked in Hewlett-Packard Labs, Palo Alto, in 1979. From 1980 to 1986, he was on the faculty of the Middle East Technical University as an Assistant Professor. In 1986, he joined Bilkent University as the chairman of the Electrical and Elec-

tronics Engineering Department and served in the founding of the department, where he is currently a Professor. In 1995, he was a Visiting Professor at Stanford University. From 1996 to 2010, he was the Provost of Bilkent University. He is presently the Rector of the same university. His current research interests include micromachined devices and microwave electronics.

Prof. Atalar was awarded the Science Award of TUBITAK in 1994. He is a Fellow of IEEE and a member of Turkish Academy of Sciences.

Hayrettin Köymen received the B.Sc. and M. Sc. degrees from the Middle East Technical University (METU), Ankara, Turkey, in 1973 and 1976, respectively, and the Ph.D. degree from Birmingham University, UK, in 1979, all in electrical engineering. He worked as a faculty member in the Marine Sciences Department (Mersin) and the Electrical Engineering Department (Ankara) of METU, from 1979 to 1990; since 1990, he has worked at Bilkent University, where he is a professor. His research activities have included underwater acoustic and ultrasonic transducer design, acoustic microscopy, ultrasonic NDT, biomedical instrumentation, mobile communications, and spectrum management.

Prof. Köymen is a fellow of IET (formerly IEE).

Hüseyin Kağan Oğuz received his B.S., M.S., and Ph.D. degrees from Bilkent University, Ankara, Turkey, in 2006, 2009, and 2014, respectively, all in electrical engineering. His graduate work focused on developing linear and nonlinear equivalent circuit models for CMUT and investigating the effects of mutual acoustic interactions in CMUT arrays. From 2009 to 2012, he was an acoustics engineer at Meteksan Defence Ind. Inc., Ankara, where he worked on modeling, fabrication, and characterization of piezoelectric transducers for commercial sonar arrays. In 2012, he joined the Bilkent University Acoustics and Underwater Technologies Research Center (BASTA) as a research engineer. Since 2014, he has been a Postdoctoral Fellow in the Edward L. Ginzton Laboratory at Stanford University.